Ceramics-Silikáty 60 (4), 285-290 (2016)
journal webpage: www.ceramics-silikaty.cz doi: 10.13168/cs.2016.0043

PHYSICAL VAPOR DEPOSITION OF Er^{3+}: $Yb_3Al_5O_{12}$ THIN FILMS FROM SOL-GEL DERIVED TARGETS

#T. HLÁSEK*, K. RUBEŠOVÁ*, V. JAKEŠ*, M. NOVÁČEK*, J. OSWALD**, P. FITL***, J. SIEGEL****, P. MACHÁČ****

*Department of Inorganic Chemistry, University of Chemistry and Technology Prague, Technická 5, Prague 6, 166 28, Czech Republic
**Institute of Physics v.v.i., Academy of Sciences of the Czech Republic, Cukrovarnická 10, Prague 6, 162 00, Czech Republic
***Department of Physics and Measurements, University of Chemistry and Technology Prague, Technická 5, Prague 6, 166 28, Czech Republic
****Department of Solid State Engineering, University of Chemistry and Technology Prague, Technická 5, Prague 6, 166 28, Czech Republic

#E-mail: hlasekt@vscht.cz

Submitted May 16, 2016; accepted August 4, 2016

Keywords: PLD, Electron beam deposition, Thin film, Ytterbium-aluminium garnet, Erbium

Although ytterbium aluminum garnets (YbAG) belong to a group of promising optical materials, no physical method of thin films deposition has been described so far. In this work we present the comparison of two valuable physical deposition techniques: pulsed laser deposition and electron beam evaporation. Erbium (Er^{3+}) doped ytterbium garnet ($Er_{0.005}Yb_{0.995})_3Al_5O_{12}$ (Er:YbAG) thin films were prepared using own sol-gel derived ceramic targets. The phase composition of the films and crystallite size were determined using X-ray diffraction. Microstructure and surface morphology were studied by scanning electron microscopy and atomic force microscopy. Deposition parameters of used methods were optimized; however, both techniques produced amorphous films with insufficient microstructure. The effect of additional annealing on the crystallinity and luminescent properties of erbium ions was studied. A pure infrared emission of Er^{3+} ions was observed only in samples prepared by pulsed laser deposition with subsequent annealing.

INTRODUCTION

Er^{3+} ion is one of the most studied activator in optical materials. With minor modifications such as the concentration of Er^{3+} or co-doping, the erbium ion can provide pure green [1], red [2] or infrared [3] emission in almost all host materials. Its transition $^4I_{13/2} \rightarrow {}^4I_{15/2}$ (the infrared emission at 1530 nm; the third telecommunication window) is now used worldwide for optical signal propagation through silica based optical fibres. To produce a material with a high efficiency of luminescence, the problem of low absorption cross section of erbium has to be solved. To overcome this phenomenon, Yb^{3+} has been successfully used as a sensitizer in many host materials such as $LiNbO_3$ [4, 5], $KY(WO_4)_2$ [6], $NaYF_4$ [7] or YAG [8, 9]. The energy transfer from ytterbium ($^2F_{5/2}$) to erbium ($^4I_{11/2}$) is highly effective when ytterbium is used as a part of the host material and not just as a co-dopant (e.g. in $Yb_3Al_5O_{12}$) [3]. However, the synthesis of a phosphor with superior luminescent properties isn't a final task for the construction of a signal amplifying device. The material should also require microstructure quality enabling the guiding of an optical signal.

Among oxide host materials, the garnets have a superior position. Garnets with a general formula $A_3B_5O_{12}$, where A is yttrium or a rare-earth metal and B is a trivalent d- or p-block metal (e.g. Al, Ga, Fe or their combination), are promising hosts for many optical applications. The main benefits of these materials are a wide transparency range, good thermal conductivity, isotropic optical properties and high thermal and chemical stability. Moreover, the garnet structure allows to modify both refractive index and lattice parameter with a composition change [10]. Thanks to these characteristics, the garnets have been used as a host material for many optical activators such as Cr^{4+} [11], Nd^{3+} [12], Ce^{3+} [13], Yb^{3+} [14] or Er^{3+} [15].

So far, methods such as liquid phase epitaxy [16], sol-gel [17], ion implantation [18] or sputtering [19] have been used to prepare the garnet based planar waveguides (yttrium aluminum garnet, YAG or yttrium iron garnet, YIG). Each method has its own advantages and limits. In our group, the Er^{3+}:$Yb_3Al_5O_{12}$ thin films have been prepared using liquid phase epitaxy (LPE) and various sol-gel techniques [20-22]. Although the LPE method produced a monocrystalline films with high optical quality, due to the potential of YbAG material, the comparison with other deposition techniques is desired.

However, YbAG thin films have not been prepared using physical deposition techniques so far. In this work, we describe Er^{3+}:$Yb_3Al_5O_{12}$ thin films prepared from physical vapors using either pulsed lased deposition or electron beam evaporation. The microstructure of prepared films was characterized by scanning electron microscope and atomic force microscope. The effect of additional annealing on the phase composition and luminescent properties of Er^{3+} ions was also studied.

EXPERIMENTAL

Target preparation

Targets with stoichiometric composition $(Er_{0.005}Yb_{0.995})_3Al_5O_{12}$ were prepared by an aqueous sol-gel method. Ytterbium acetate was dissolved in diluted acetic acid (volume ratio acetic acid: H_2O = 15:85); ethylenediaminetetraacetic acid (EDTA) was added. To fully dissolve EDTA, pH was adjusted by ammonia up to 6. Then triethanolamine (TEA) was added to the ytterbium solution. Finally, Al^{3+} and Er^{3+} ions were introduced by adding an aqueous solution of aluminium chloride (0.1 mol·l^{-1}) and solid anhydrous erbium acetate, respectively. The molar ratio between EDTA, TEA and metals was 1:1:1. The final solution was gelled at 80°C for 2 h. Clear, slightly yellow gel was dried for 2 h at 250°C. The dried gel was calcined at 500°C and 900°C for 2 h in an ambient atmosphere. The precursor powder was uniaxially pressed into pellets by a pressure of 500 MPa for 1 min. Finally, the pellets were sintered at 1300°C for 168 h in an ambient atmosphere. For more details see our previous study [3].

Electron beam evaporation

Er^{3+}:$Yb_3Al_5O_{12}$ layers were deposited by vacuum evaporation using LEYBOLD-HERAEUS Univex 450 device with an electron gun source. The evaporation was performed at room temperature at a rate of 0.5 nm·s^{-1}. Distance between the source material and a sapphire substrate was 135 mm. Accelerating voltage was 9.5 kV limiting the current of electron beam to 80 mA. The pressure inside the working chamber was constant during the deposition at the level of 2×10^{-6} mbar. Both deposition rate and thickness of deposited material were controlled in-situ by a crystal oscillator. Under these evaporation conditions, the resulting Er^{3+}:$Yb_3Al_5O_{12}$ layers were about 200, 700 and 3000 nm thick (measured by AFM [23]).

In the case of 3 μm thick films, the deposition process had to be accomplished in two steps by adding the source material. Otherwise, there has been a risk of damage of an electron gun hole by electron beam because of a rapid loss of deposited material. When refilling the source material, it was necessary to aerate the apparatus.

Pulsed laser deposition

The samples were prepared by a PLD system [24] equipped with a turbo pumped high vacuum chamber (limit pressure 1×10^{-6} mbar) utilising Nd:YAG laser Quantel Brilliant with module for the generation of 4th harmonic frequency – 266 nm, repetition rate 10 Hz, pulse duration 4 ns, laser pulse energy 40 mJ. The laser beam was focused by optics to achieve a suitable energy density of 2 J·cm^{-2} on the source material target. The target and substrate were rotating during deposition to avoid crater effects and to achieve good thickness homogeneity on the substrate. The distance between source and target was 45 mm.

Sample characterization

The phase composition of the prepared samples was determined by X-ray diffraction (XRD). The device used was Bruker AXS D2 Phaser powder diffractometer with parafocusing Bragg–Brentano geometry using CoK_a radiation (l = 1.7890 Å, U = 30 kV, I = 10 mA). Data evaluation was performed in the software package HighScore Plus. Scanning electron microscopy (SEM) was carried out using Vega 3 LMU (TESCAN) equipped with an EDS analyzer INCA 350 (Oxford Instruments). The morphology of samples surface was determined by atomic force microscopy (AFM) using Ntegra Spectra (NT-MDT). Surface scans were performed in a tapping (semi-contact) mode. Cantilevers with a strain constant of 1.5 kN·m^{-1} equipped with a standard silicon tip (curvature radius < 10 nm) were used for all measurements. The photoluminescence spectra of the prepared films were collected within a range of 1440 - 1650 nm at room temperature. A semiconductor laser POL 4300 emitting at 980 nm was used for the excitation of electrons (power used was 65 mW, 10 W·cm^{-2}). The luminescence radiation was detected by a two-step-cooled Ge detector J16 (Teledyne Judson Technologies). To scoop specific wavelengths, a double monochromator SDL-1 (LOMO) was used. Synchronous detection technique was implemented by chopping the laser beam at a modulation frequency of about 35 Hz, and by employing a lock-in amplifier (EG&G 5205). For evaluation, all luminescence spectra were transformed to the base level and normalized using a standard measurement.

RESULTS AND DISCUSSION

Firstly, both deposition methods were optimized to achieve sufficiently thick films. With respect to refractive indexes of YbAG and substrates (SiO_2 or Al_2O_3), the thickness of 700 nm and higher would be suitable for light propagation. Other important parameters for the construction of a light amplifying device are surface roughness, microstructure and photoluminescent properties. All these aspects were studied and the results are given below.

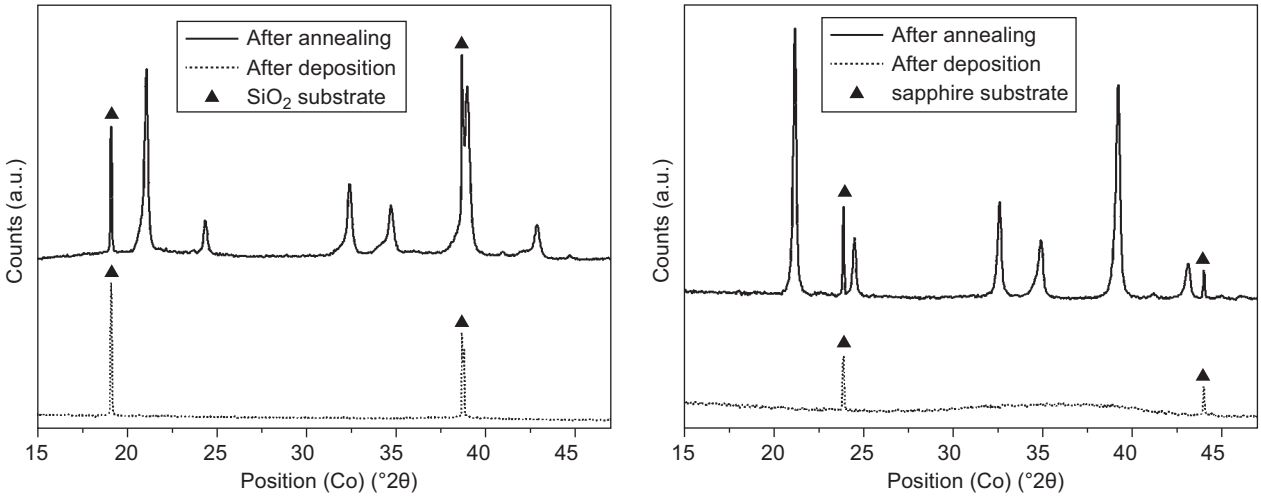

a) pulsed laser deposition b) electron beam evaporation

Figure 1. XRD patterns of as-deposited and annealed films prepared by PLD (a) and electron beam evaporation (b).

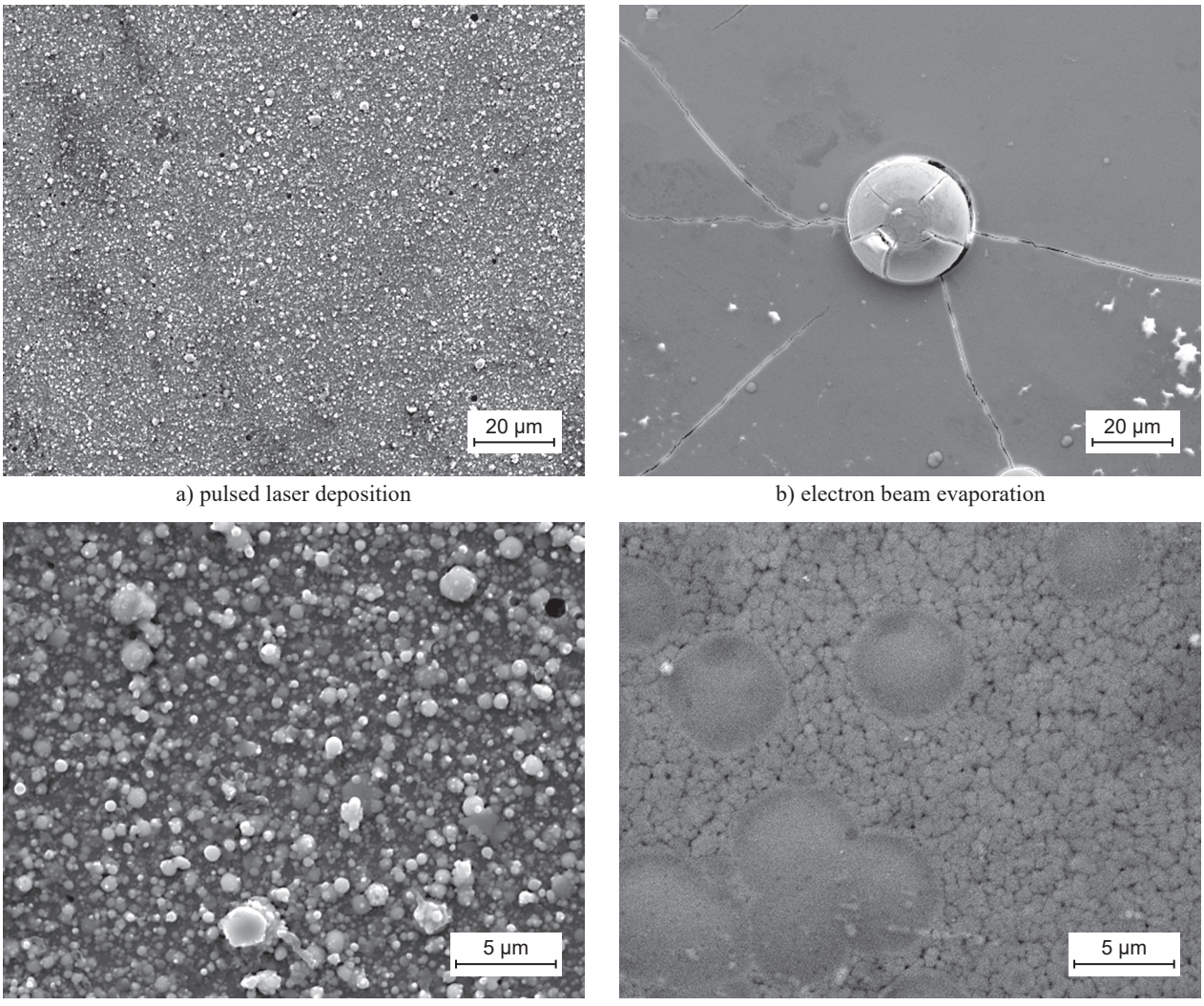

a) pulsed laser deposition b) electron beam evaporation

c) pulsed laser deposition d) electron beam evaporation

Figure 2. SEM images of films prepared by PLD (a,c) and electron beam evaporation (b,d) with magnification 1 000× and 5 000× for (a, b) and (c, d), respectively.

It can be seen from X-ray diffraction patterns of the films after deposition (Figure 1) that the as-deposited films were amorphous and only diffraction lines of substrates were visible in both used deposition techniques. Because of this phenomenon, all samples were additionally annealed (1000°C for 1 h) to achieve crystalline films. Diffraction patterns of the annealed samples show the single phase composition of the films prepared by both deposition methods. The only visible phase was $Yb_3Al_5O_{12}$ (PDF 01-073-1369). From diffraction lines broadening, the crystallite size and micro-strain can be estimated using Williamson–Hall method. For the construction of Williamson–Hall plot only (211), (220), (321) and (400) diffraction lines were used (sufficient intensity, no overlap with substrate peaks). The estimated crystallite size was 46 and 58 nm for films prepared using PLD and electron beam evaporation, respectively. Identical heat-treatment was used for both samples, both values of micro-strain were about 0.5 %. It also indicates that the use of different substrate (either SiO_2 or Al_2O_3) had no influence on the micro-strain after heat treatment.

From electron scanning microscopy (Figure 2), it is clearly visible that the microstructure of samples prepared by PLD and electron beam evaporation differs considerably. Although the phase composition of targets used for both methods was identical, the microstructure of resulted films was driven by different kinetics of nucleation and different deposition mechanisms. PLD produced layers with uniform but rough surface (Figure 2a, c). On the other hand, the e-beam films had a smooth surface combined with isolated spherical particles connected by cracks through the layer (Figure 2b, d). Figure 2c and d show the details of the smoothest sections of PLD and e-beam film (5 000 ´ magnification), respectively. The PLD film exhibited relatively homogeneous grain growth with nucleation in a volume of deposited amorphous layer resulting in rough surface. On the other hand, two different nucleation mechanisms can be seen in the e-beam film. In higher magnification (Figure 2d), the circular areas with lower porosity suggest the nucleation on the substrate surface and the volume nucleation can be seen in the porous rest of the film. This phenomenon and the presence of spherical particles (Figure 2b) suggest the inhomogeneous deposition.

The surface morphology was also observed using atomic force microscopy. The 3D images are displayed in Figure 3. The results are in good agreement with SEM observations. The arithmetic average (R_a) and root mean squared (R_{RMS}) roughness of the PLD film was 120 nm and 153 nm, respectively. Thanks to the character of e-beam films surface, the determination of R_a and R_{RMS} strongly depends on the actual position of the scan. The roughness of the smooth parts was about 5 nm (R_a); however, the height of the spherical artifacts was about 1 μm (even higher artifacts were observed, but not measured by AFM).

The microstructure and surface morphology of prepared film was insufficient for light propagation due to the impossibility to establish optical contact. The quality of the film surface is one of the key parameters for the construction of a planar waveguide. In our previous works, we prepared films with the same composition by liquid phase epitaxy and sol-gel method. The surface roughness (R_a) of these films was only 0.2 nm and 1.9 nm, respectively and the films were planar waveguides at wavelength of 1550 nm in both cases. However, methods presented in this work could produce films with a better surface morphology when a more advanced experimental setup is used.

Besides a suitable thickness and microstructure, the efficient infrared emission is needed for the construction of a light amplifying device. Erbium with its Er^{3+}: $^4I_{13/2} \rightarrow {}^4I_{15/2}$ transition (maximum at around 1530 nm) is commonly used for signal transmission through silica fibers. Figure 4 shows the emission spectra of this transition for the PLD film after deposition and also after the additional annealing. It can be seen that the erbium ions had no radiative transition in amorphous matrix (as-deposited film). After the crystallization, the spectrum exhibits characteristic bands for Er^{3+} in the YbAG

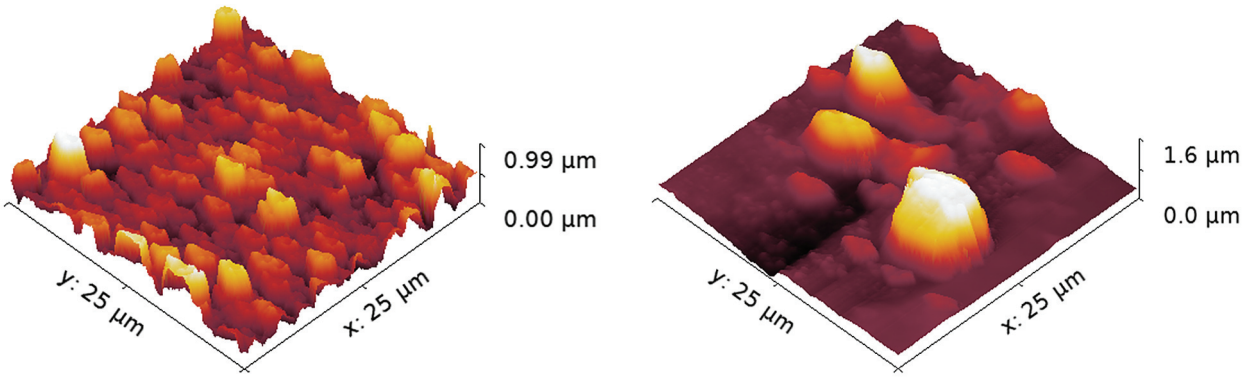

a) pulsed laser deposition

b) electron beam evaporation

Figure 3. Surface morphology of prepared films – 3D images from AFM.

matrix. The overlapping particular emissions form broad maxima at wavelengths about 1460 nm and 1530 nm. This broad emission is characteristic for nano-crystalline materials where the emission is strongly influenced by different symmetry of erbium surroundings close to the grain boundaries. This fact is in good agreement with the crystallite size calculated from XRD patterns. Films prepared by the electron beam evaporation did not exhibit infrared emission even after subsequent annealing. This phenomenon could be caused by erbium cluster formation during the deposition or by an inhomogeneous transfer of ions during deposition. Both mechanisms would result in this type of behavior, but there is no direct proof for either due to the low concentration of erbium. The e-beam sample was analyzed by XPS (X-Ray photoelectron spectroscopy), however the presence of neither Er^{3+} nor Er^0 was detected. Another reason for the lack of infrared erbium emission could be the presence of iron impurities. Iron impurities were detected by the EDS measurement in all samples (starting target, PLD and e-beam), but the iron concentration in the e-beam films was significantly higher. The high concentration of iron in the e-beam samples could be due to contamination from a source material holder which contains iron.

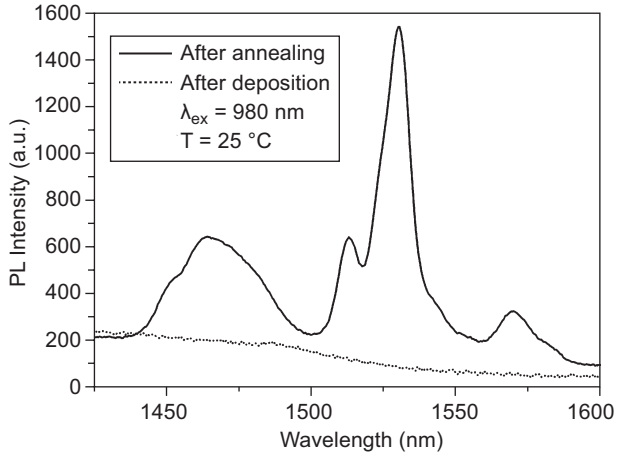

Figure 4. The emission spectra of Er^{3+}: $^4I_{13/2} \rightarrow {}^4I_{15/2}$ transition in PLD sample after deposition and after subsequent annealing.

CONCLUSIONS

The polycrystalline films with a single-phase garnet structure were successfully prepared by two physical vapor deposition methods: pulsed laser deposition and electron beam evaporation. Sol-gel derived ceramics with stoichiometry $(Er_{0.005}Yb_{0.995})_3Al_5O_{12}$ (Er:YbAG) was used as a target material. The experimental conditions were adjusted to produce films with a thickness about 700 nm. To achieve a single-phase crystalline structure, the additional annealing (1000°C for 1 h) was necessary. The film prepared by PLD exhibited a homogeneous but rough surface with R_a about 120 nm. The film deposited using the electron beam evaporation was smoother, but artifacts such as cracks or spherical particles appeared due to inhomogeneous deposition. The microstructure of prepared films could be further optimized by employing more advanced deposition apparatus (e.g. with a substrate heating). The sample deposited using PLD with a subsequent annealing exhibited a pure infrared emission of Er^{3+}: $^4I_{13/2} \rightarrow {}^4I_{15/2}$ transition with a broad maximum around 1530 nm. Despite the additional annealing, the films prepared using the electron beam evaporation did not show any emission of erbium ions. Although the used physical vapor deposition methods were not successful at this multi-cation waveguide preparation, we plan to employ other more suitable equipment to achieve this goal.

Acknowledgements

This work was financially supported from specific university research (MSMT No 20/2016)

REFERENCES

1. Li Z.P., Dong B., He Y.Y., Cao B.S., Feng Z.Q. (2012): Selective enhancement of green upconversion emissions of Er^{3+}:$Yb_3Al_5O_{12}$ nanocrystals by high excited state energy transfer with Yb^{3+}-Mn^{2+} dimer sensitizing. *Journal of Luminescence*, *132*(7), 1646-1648. doi:10.1016/j.jlumin.2012.02.034
2. Xu C., Yang Q., Ren G., Liu Y. (2010): Pure red upconversion emission from $Yb_3Al_5O_{12}$ phase doped with high Er^{3+} concentration. *Journal of Alloys and Compounds*, *503*(1), 82-85. doi:10.1016/j.jallcom.2009.12.189
3. Hlásek T., Rubešová K., Jakeš V., Jankovský O., Oswald J. (2014): Infrared luminescence in Er^{3+}:$Yb_3Al_5O_{12}$ bulk ceramics prepared by sol-gel method. *Journal of the European Ceramic Society*, *34*(15), 3779-3782. doi:10.1016/j.jeurceramsoc.2014.06.017
4. Jelinek M., Oswald J., Kocourek T., Rubesova K., Nekvindova P., Chvostova D., Dejneka A., Zelezny V., Studnicka V., Jurek K. (2013): Optical properties of laser-prepared Er-and Er,Yb-doped $LiNbO_3$ waveguiding layers. *Laser Physics*, *23*(10), 105819. doi:10.1088/1054-660X/23/10/105819
5. Shim J.B., Yoshimoto N., Yoshizawa M., Yoon D.H. (2001): Structural characteristics of Er doped $LiNbO_3$ thin films grown by the liquid phase epitaxy method. *Crystal Research and Technology*, *36*(11), 1209-1214. doi:10.1002/1521-4079(200111)36:11<1209::AID-CRAT1209>3.0.CO;2-D
6. García-Revilla S., Valiente R., Romanyuk Y.E., Pollnau M. (2008): Temporal dynamics of upconversion luminescence in Er^{3+}, Yb^{3+} co-doped crystalline $KY(WO_4)_2$ thin films. *Journal of Luminescence*, *128*(5–6), 934-936. doi:10.1016/j.jlumin.2007.12.025
7. Huang X., Hu G., Xu Q., Li X., Yu Q. (2014): Molten-salt synthesis and upconversion of hexagonal $NaYF_4$:Er^{3+}:Yb^{3+} micro-/nano-crystals. *Journal of Alloys and Compounds*,

616(0), 652-661. doi:10.1016/j.jallcom.2014.07.067
8. Garskaite E., Lindgren M., Einarsrud M.-A., Grande T. (2010): Luminescent properties of rare earth (Er, Yb) doped yttrium aluminium garnet thin films and bulk samples synthesised by an aqueous sol–gel technique. *Journal of the European Ceramic Society*, *30*(7), 1707-1715. doi:10.1016/j.jeurceramsoc.2010.01.001
9. Zhou J., Zhang W., Huang T., Wang L., Li J., Liu W., Jiang B., Pan Y., Guo J. (2011): Optical properties of Er,Yb co-doped YAG transparent ceramics. *Ceramics International*, *37*(2), 513-519. doi:10.1016/j.ceramint.2010.09.031
10. Tien P.K., Martin R.J., Blank S.L., Wemple S.H., Varnerin L.J. (1972): Optical waveguides of single-crystal garnet films. *Applied Physics Letters*, *21*(5), 207-209. doi:10.1063/1.1654346
11. Xu X.D., Zhao Z.W., He X.M., Song P.X., Zhou G.Q., Xu J., Deng P.Z. (2004): Growth and thermal properties of Cr^{4+}: YbAG single crystal. *Materials Letters*, *58*(25), 3153-3155. doi:10.1016/j.matlet.2004.05.062
12. Yagi H., Yanagitani T., Takaichi K., Ueda K.-i., Kaminskii A.A. (2007): Characterizations and laser performances of highly transparent Nd^{3+}:$Y_3Al_5O_{12}$ laser ceramics. *Optical Materials*, *29*(10), 1258-1262. doi:10.1016/j.optmat.2006.01.033
13. Murai S., Verschuuren M.A., Lozano G., Pirruccio G., Koenderink A.F., Rivas J.G. (2012): Enhanced absorption and emission of $Y_3Al_5O_{12}$:Ce^{3+} thin layers prepared by epoxide-catalyzed sol-gel method. *Optical Materials Express*, *2*(8), 1111-1120. doi:10.1364/OME.2.001111
14. Pelenc D., Chambaz B., Chartier I., Ferrand B., Wyon C., Shepherd D.P., Hanna D.C., Large A.C., Tropper A.C. (1995): High slope efficiency and low threshold in a diode-pumped epitaxially grown Yb:YAG waveguide laser. *Optics Communications*, *115*(5–6), 491-497. doi:10.1016/0030-4018(95)00015-Z
15. Xu H.L., Kröll S. (2005): Upconversion dynamics in Er^{3+}-doped YAG. *Journal of Luminescence*, *111*(3), 191-198. doi:10.1016/j.jlumin.2004.08.047
16. Ferrand B., Pelenc D., Chartier I., Wyon C. (1993): Growth by LPE of Nd: YAG single crystal layers for waveguide laser applications. *Journal of Crystal Growth*, *128*(1–4, Part 2), 966-969. doi:10.1016/S0022-0248(07)80079-0
17. Wu Y.C., Parola S., Marty O., Villanueva-Ibanez M., Mugnier J. (2005): Structural characterizations and waveguiding properties of YAG thin films obtained by different sol-gel processes. *Optical Materials*, *27*(9), 1471-1479. doi:10.1016/j.optmat.2005.03.004
18. Chen F., Tan Y., Jaque D. (2009): Ion-implanted optical channel waveguides in neodymium-doped yttrium aluminum garnet transparent ceramics for integrated laser generation. *Optics Letters*, *34*(1), 28-30. doi:10.1364/OL.34.000028
19. Toshihiro S., Takehiko U. (1996): Preparation of Ce-Substituted Yttrium Iron Garnet Films for Magneto-Optic Waveguide Devices. *Japanese Journal of Applied Physics*, *35*(9R), 4689. doi:10.1143/JJAP.35.4689
20. Hlásek T., Rubešová K., Jakeš V., Nekvindová P., Oswald J., Kučera M., Hanuš M. (2015): Influence of gallium on infrared luminescence in Er^{3+} doped $Yb_3Al_{5-y}Ga_yO_{12}$ films grown by the liquid phase epitaxy. *Journal of Luminescence*, *164*(0), 90-93. doi:10.1016/j.jlumin.2015.03.030
21. Hlásek T., Rubešová K., Jakeš V., Nekvindová P., Kučera M., Daniš S., Veis M., Havránek V. (2015): Structural and waveguiding characteristics of Er^{3+}:$Yb_3Al_{5-y}Ga_yO_{12}$ films grown by the liquid phase epitaxy. *Optical Materials*, *49*, 46-50. doi:10.1016/j.optmat.2015.08.025
22. Rubešová K., Hlásek T., Jakeš V., Matějka P., Oswald J., Holzhauser P. (2014): Ytterbium and erbium derivatives of 2-methoxyethanol and their use in the thin film deposition of Er-doped $Yb_3Al_5O_{12}$. *Journal of Sol-Gel Science and Technology*, *70*(1), 142-148. doi:10.1007/s10971-014-3283-y
23. Siegel J., Krajcar R., Kolská Z., Hnatowicz V., Švorčík V. (2011): Annealing of gold nanostructures sputtered on polytetrafluoroethylene. *Nanoscale Research Letters*, *6*(1), 1-6. doi:10.1186/1556-276X-6-588
24. Swanepoel R. (1983): Determination of the thickness and optical constants of amorphous silicon. *Journal of Physics E: Scientific Instruments*, *16*(12), 1214. doi:10.1088/0022-3735/16/12/023